

1

2

Greening of the Earth and its drivers

3 Zaichun Zhu^{1,2}, Shilong Piao^{1,2*}, Ranga B. Myneni³, Mengtian Huang², Zhenzhong
4 Zeng², Josep G. Canadell⁴, Philippe Ciais⁵, Stephen Sitch⁶, Pierre Friedlingstein⁷,
5 Almut Arneth⁸, Chunxiang Cao⁹, Lei Cheng¹⁰, Etsushi Kato¹¹, Charles Koven¹², Yue
6 Li², Xu Lian², Yongwen Liu², Ronggao Liu¹³, Jiafu Mao¹⁴, Yaozhong Pan¹⁵, Shushi
7 Peng², Josep Peñuelas^{16,17}, Benjamin Poulter^{18,19}, Thomas A. M. Pugh⁸, Benjamin D.
8 Stocker²⁰, Nicolas Viovy⁵, Xuhui Wang², Yingping Wang²¹, Zhiqiang Xiao²², Hui
9 Yang², Sönke Zaehle²³, Ning Zeng²⁴

10

11 ¹ Institute of Tibetan Plateau Research, Center for Excellence in Tibetan Earth Science,
12 Chinese Academy of Sciences, Beijing 100085, China.

13 ² Sino-French Institute for Earth System Science, College of Urban and Environmental
14 Sciences, Peking University, Beijing 100871, China

15 ³ Department of Earth and Environment, Boston University, Boston, Massachusetts
16 02215, USA

17 ⁴ Global Carbon Project, CSIRO Oceans and Atmosphere, GPO Box 3023, Canberra,
18 ACT 2601, Australia

19 ⁵ Laboratoire des Sciences du Climat et de l'Environnement (LSCE), CEA CNRS UVSQ,
20 91191 Gif Sur Yvette, France.

21 ⁶ College of Engineering, Computing and Mathematics, University of Exeter, Exeter EX4
22 4QF, UK.

⁷ College of Engineering, Mathematics and Physical Sciences, University of Exeter,

Exeter EX4 4QF, UK

⁸ Institute of Meteorology and Climate Research, Atmospheric Environmental Research,

Karlsruhe Institute of Technology, 82467 Garmisch-Partenkirchen, Germany.

⁹ State Key Laboratory of Remote Sensing Science, Institute of Remote Sensing and

Digital Earth, Chinese Academy of Sciences, Beijing 100101, China

¹⁰ CSIRO Land and Water, Black Mountain, Canberra, ACT 2601, Australia

¹¹ Institute of Applied Energy (IAE), Minato-ku, Tokyo 105-0003, Japan

¹² Earth Sciences Division, Lawrence Berkeley National Lab, 1 Cyclotron Road,

Berkeley, CA 94720, USA

¹³ Institute of Geographic Sciences and Natural Resources Research, Chinese Academy of

Sciences, Beijing, 100101, China

¹⁴ Climate Change Science Institute and Environmental Sciences Division, Oak Ridge

National Laboratory, Oak Ridge, TN, USA

¹⁵ College of Resources Science & Technology, State Key Laboratory of Earth

Processes and Resource Ecology, Beijing Normal University, Beijing 100875, China

¹⁶ CSIC, Global Ecology Unit CREAF-CEAB-UAB, Cerdanyola del Vallès, 08193

Catalonia, Spain

1 ¹⁷ CREAM, Cerdanyola del Vallès, 08193 Catalonia, Spain

2 ¹⁸ Montana State University, Institute on Ecosystems and the Department of Ecology,

3 Bozeman, Montana 59717, USA.

4 ¹⁹ Laboratoire des Sciences du Climat et de l'Environnement (LSCE), CEA CNRS

5 UVSQ, 91191 Gif Sur Yvette, France.

6 ²⁰ Department of Life Sciences, Imperial College London, Silwood Park, Ascot, SL5

7 7PY, UK

8 ²¹ CSIRO Ocean and Atmosphere, PMB #1, Aspendale, Victoria 3195, Australia

9 ²² State Key Laboratory of Remote Sensing Science, School of Geography, Beijing

10 Normal University, Beijing 100875, China

11 ²³ Max-Planck-Institut für Biogeochemie, P.O. Box 600164, Hans-Knöll-Str. 10, 07745

12 Jena, Germany

13 ²⁴ Department of Atmospheric and Oceanic Science, University of Maryland, College

14 Park, MD 20742, US

15 *Correspondence to: Shilong Piao, slpiao@pku.edu.cn

16

17

18

19

Greening of the Earth and its drivers

Global environmental change is rapidly altering the dynamics of terrestrial vegetation with consequences for the functioning of the Earth system and provision of ecosystem services^{1,2}. Yet how global vegetation is responding to the changing environment is not well established. Here we use 3 long-term satellite leaf area index (LAI) records and 10 global ecosystem models to investigate four key drivers of LAI trends during 1982-2009. We show a persistent and widespread increase of growing season integrated LAI (greening) over 25 to 50% of the global vegetated area, whereas less than 4% of the globe shows decreasing LAI (browning). Factorial simulations with multiple global ecosystem models suggest that CO₂ fertilization effects explain 70% of the observed greening trend, followed by nitrogen deposition (9%), climate change (8%) and land cover change (LCC) (4%). CO₂ fertilization effects explain most of the greening trends in the tropics, while climate change resulted in greening of the high latitudes and the Tibetan Plateau. LCC contributed most to the regional greening observed in Southeast China and Eastern United States. The regional effects of unexplained factors suggest that the next generation of ecosystem models will need to explore the impacts of forest demography, differences in regional management intensities for cropland and pastures, and other emerging productivity constraints such as phosphorus availability.

1 **Main**

2 Changes in vegetation greenness have been reported at regional and continental scales
3 based on forest inventory and satellite measurements³⁻⁸. Long-term changes in
4 vegetation greenness are driven by multiple interacting biogeochemical drivers and
5 land use effects⁹. Biogeochemical drivers include the fertilization effect of elevated
6 atmospheric CO₂ concentration (eCO₂), regional climate change (temperature,
7 precipitation, and radiation), and varying rates of nitrogen deposition. Land use related
8 drivers involve changes in land cover and in land management intensity, including
9 fertilization, irrigation, forestry and grazing¹⁰. None of these driving factors can be
10 considered in isolation given their strong interactions with one another. Previously, a
11 few studies had investigated the drivers of global greenness trends^{6,7,11} with a limited
12 number of models and satellite observations, which prevented an appropriate
13 quantification of uncertainties¹².

14
15 Here, we investigate trends of Leaf Area Index (LAI) and their drivers for the period
16 1982 to 2009 utilizing 3 remotely sensed data sets (GIMMS3g, GLASS and GLOMAP)
17 and outputs from 10 ecosystem models run at global extent (see Supplementary
18 Information). We use the growing season integrated leaf area index (LAI hereafter –
19 Methods) as the variable of our study. We first analyze global and regional LAI trends
20 for the study period and differences between the 3 data sets. Using modeling results,
21 we then quantify the contributions of CO₂ fertilization, climatic factors, nitrogen
22 deposition and LCC to the observed trends.

1 Trends from the 3 long-term satellite LAI data sets consistently show positive values
2 over a large proportion of the global vegetated area since 1982 (Fig. 1). The global
3 greening trend estimated from the three data sets is $0.068 \pm 0.045 \text{ m}^2\text{m}^{-2}\text{yr}^{-1}$. The
4 GIMMS LAI3g data set that includes recent data up to 2014, shows a continuation of
5 the trend from the 1982-2009 period (Fig.1 and Fig. S3). The regions with the largest
6 greening trends, consistent across the 3 data sets, are in Southeast North America,
7 Northern Amazon, Europe, Central Africa and Southeast Asia. The GLASS LAI data
8 shows the most extensive statistically significant greening (Mann-Kendal test, $p < 0.05$)
9 over 50% of vegetated lands, followed by GLOBMAP LAI (43%) and GIMMS LAI3g
10 (25%). All 3 LAI data sets also consistently show a decreasing LAI trend (browning)
11 over less than 4% of global vegetated land – these are observed in Northwest North
12 America and Central South America. Analyses of the changes in observed maximum
13 LAI also show similar widespread greening trends (Section S8).

14

15 We compare satellite-based LAI anomalies with LAI anomalies simulated by 10 global
16 ecosystem models driven by eCO_2 (+46 ppm over the study period), climate, nitrogen
17 deposition and LCC (Section S7). Multi-Model Ensemble Mean (MMEM) LAI
18 anomalies with all these drivers considered, generally agree with averaged satellite
19 observations at the global scale ($r=0.85$, $p < 0.01$; Fig. 2a). The trend in MMEM LAI
20 anomalies ($0.062 \text{ m}^2\text{m}^{-2}\text{yr}^{-1}$) is within the range of estimates from the 3 satellite data
21 sets. The model simulations suggest that increasing gross primary productivity,
22 although partly neutralized by increasing autotrophic respiration, and decreasing carbon

1 loss due to fires are responsible for the increasing LAI during 1982 to 2009 (Section
2 S9). The spatial pattern of LAI trends also matches well between satellite data and
3 MMEM simulations (Fig. 3a, b). Consistent greening trends between models and
4 observations are seen in Fig. 3 across the Southeast United States, the Amazon basin,
5 Europe, central Africa, Southeast Asia and Australia. However, satellite LAI and
6 MMEM results show different magnitude (or sign) of trends in the Southwestern United
7 States, Southern South American countries, and Mongolia, indicating that models may
8 be over-sensitive to trends in precipitation (Section S10).

9
10 We used an optimal fingerprint detection method¹³ to assess the ability of the models to
11 simulate observed patterns of LAI response to eCO₂, climate change, nitrogen
12 deposition and LCC. We regressed the observed 2-year mean global average LAI time
13 series against the MMEM simulated LAI reflecting the effects of single drivers, based
14 on factorial runs where only one driver is varied at the time. A residual consistency
15 test¹³ suggests no inconsistency between the regression residuals and the model
16 simulated internal variability in the absence of forcing (Methods), indicating that the
17 fingerprint detection method is suitable for detection and attribution at the global scale
18 (Fig. 2b). The 95% confidence intervals of the scaling factors of CO₂ fertilization (best
19 estimates of scaling factor $\beta = 1.03$, 95% confidence interval [0.84,1.23]) and climate
20 change ($\beta = 1.06$, [0.55,1.64]) are not only above zero but also span unity, which
21 means that the modeled signals from these two drivers are successfully detected and
22 suitable for attribution (Fig. 2b). The fingerprints of nitrogen deposition and LCC

1 effects on the trend of LAI remain confounded with internal variability and cannot be
2 clearly detected (not shown).

3

4 Globally, the model factorial simulations suggest that CO₂ fertilization explains the
5 largest contribution to the satellite observed LAI trend ($70.1 \pm 29.4\%$, $0.048 \pm 0.020 \text{ m}^2\text{m}^{-2}\text{yr}^{-1}$),
6 followed by nitrogen deposition ($8.8 \pm 11.8\%$, $0.006 \pm 0.008 \text{ m}^2\text{m}^{-2}\text{yr}^{-1}$), climate
7 change ($8.1 \pm 20.6\%$, $0.006 \pm 0.014 \text{ m}^2\text{m}^{-2}\text{yr}^{-1}$) and LCC ($3.7 \pm 14.7\%$, $0.003 \pm 0.010 \text{ m}^2\text{m}^{-2}\text{yr}^{-1}$)
8 (Fig. 2c). The contributions of CO₂ fertilization and climate change are reliable
9 according to the optimal fingerprint analysis, while the effects of LCC and nitrogen
10 deposition should be interpreted with caution. Our estimation of CO₂ fertilization
11 effects on vegetation growth is more prominent than Los⁶, which is likely due to the
12 different attribution approaches. When using only those ecosystem models (5 out of 10)
13 that incorporate N limitations and nitrogen deposition effects (Table S1), the fraction of
14 the LAI trend that is unambiguously attributed to CO₂ fertilization is slightly smaller
15 ($66.2 \pm 13.2\%$, $0.045 \pm 0.009 \text{ m}^2\text{m}^{-2}\text{yr}^{-1}$) than when using models that ignore nitrogen
16 processes ($75.0 \pm 42.6\%$, $0.051 \pm 0.029 \text{ m}^2\text{m}^{-2}\text{yr}^{-1}$). This suggests that although
17 incorporating nitrogen in ecosystem models does not significantly (t-test, $p < 0.05$)
18 change the contribution of the CO₂ fertilization effect to the global trend of LAI, it
19 reduces the spread of model simulations (F-test, $p < 0.05$).

20

21 Vegetation leaf area changes result from interacting factors, but factorial simulations
22 help to attribute a dominant factor for the observed changes. Our analyses show that

1 the CO₂ fertilization effect has a rather spatially uniform effect on the positive LAI
2 trends. The modeled relative increases in global mean LAI due to CO₂ fertilization
3 alone is about 4.7-9.5% (or 10.2-20.7% per 100ppm) during 1982 to 2009, which is
4 comparable to measurements from the Free-Air CO₂ Enrichment (FACE) experiments
5 (0.3-11.1%, or 0.6-24.1% per 100ppm)¹⁴. However, no FACE experiment covered
6 tropical forests, where models suggest that eCO₂ is the dominant factor of the recent
7 LAI trend (Fig. 3c, d). The spatial pattern is consistent with previous analyses¹⁵ that
8 posited large absolute LAI increases due to eCO₂ in the tropics, in the absence of
9 temperature, water and nitrogen limitations¹⁶, and large relative LAI increases due to
10 eCO₂ in arid regions, where eCO₂ is expected to increase water use efficiency of plants
11 (Fig. S12)¹⁷. A simple theoretical model^{17,18} was used to diagnose the response of leaf
12 level carbon assimilation to the observed 46 ppm increase of CO₂ over the study period,
13 including the effect of vapor pressure deficit trends and stomatal closure. This model
14 gave a similar relative response of carbon assimilation to eCO₂ as the ecosystem models
15 did for LAI (Section S12).

16

17 Climate change explains about $8.1 \pm 20.1\%$ of the observed positive LAI trend, but
18 unlike eCO₂ effects, climatic effects are negative in some regions. Although detected
19 by the optimal fingerprint model, the effects of climate change are not consistent
20 between models, and may even be opposite in individual model simulations. Overall,
21 climate change has dominant contributions to the greening trend over 28.4% of the
22 global vegetated area (Fig. 3c, d). Positive effects of climate change in the Northern

1 high latitudes and the Tibetan Plateau are attributed to rising temperature, which
2 enhances photosynthesis and lengthens the growing season⁵, whereas the greening of
3 the Sahel and South Africa are primarily driven by increasing precipitation (Fig. S13).
4 South America is the only continent where negative climate effects were statistically
5 significant (Fig. S10 and Fig. S11b). This is particularly important due to the role of the
6 Amazon forests in the global carbon cycle^{19,20}. Ecosystem models may tend to
7 overestimate the responses of vegetation growth to precipitation¹² (Section S10) which
8 is one of the reasons why the fate of the Amazon forests continues to be debated¹⁰.

9
10 Considerable evidence points to nitrogen limitation of vegetation growth over many
11 parts of the Earth²¹, with local alleviation by nitrogen deposition in boreal and
12 temperate regions^{22,23}. Our analyses suggest that nitrogen deposition explains $8.8 \pm 11.8\%$
13 of the LAI trend at the global scale. However, this result is uncertain because only two
14 models in the ensemble specifically performed factorial simulations with and without
15 nitrogen deposition. A slightly negative trend in nitrogen deposition effect was
16 observed in North America and Europe, where nitrogen deposition rates have stabilized
17 or even declined during the last three decades^{24,25}.

18
19 LCC is a dominant driver of LAI greening only over 9.6% of the global vegetated area,
20 mainly in Southeast China and Southeast United States. Models produce negative LCC
21 effects on LAI trends in tropical and southern temperate regions where deforestation
22 occurred (Fig. S11d)²⁶. The individual effect of LCC seems however to be outweighed
23 by other factors in these regions, and thus does not appear to be dominant. Trends of

1 the LCC effect simulated by ecosystem models differ significantly in magnitude, and
2 sometimes also in sign. This could be due to differences in model assumptions relating
3 to whether the productivity of secondary vegetation is smaller or larger than that of the
4 vegetation it replaces.

5

6 At the global scale, the observed LAI trend can be largely accounted for by CO₂, climate,
7 nitrogen deposition and LCC. However, at regional scales, other factors (OF) not
8 considered in models such as forest management, grazing, changes in cultivation
9 practices and varieties, irrigation and disturbances such as storms and insect attacks,
10 can be a cause of mismatch between observed and simulated LAI trends. The patterns
11 of the effect of other factors were estimated as a residual, by subtracting the simulated
12 trend caused by factors explicitly modeled from the observed local LAI trend. OF
13 contributes the most to the observed LAI trend over 25.0% (increase) and 5.3%
14 (decrease) of the vegetated area (Fig. 3d). OF can also encompass non-modeled
15 processes such as plant diversity within a type of vegetation, hydrological and nutrient
16 liberation during permafrost thawing, phosphorus and potassium limitations, access to
17 ground water by deep roots, and rigid discretization of the simulated vegetation into
18 few plant functional types. Further, uncertainties in existing model parameterization
19 and structure (Section S7) and biases from the remote sensing data sets (Section S6)
20 can cause a mismatch between simulated and observed LAI trends. Interestingly,
21 positive effects tentatively attributed to OF are mainly found in areas of intensive
22 ecosystem management such as northeast China, Europe, and India²⁷. Negative OF

1 effects are mainly found in northern high latitudes where most models lack a
2 representation of regionally important ecosystems (peatlands, wetlands) as well as of
3 specific disturbances^{28,29}.

4

5 Understanding the mechanisms behind LAI trends is a first, yet critical, step towards
6 better understanding the influence of human actions on terrestrial vegetation, and
7 towards improving future projections of vegetation dynamics. Utilizing three LAI data
8 sets, an ensemble of 10 ecosystem models, and a fingerprinting technique, we assessed
9 the consistency of observed greening and browning patterns with the effects of key
10 environmental drivers. The use of a 10-model ensemble increases confidence in the
11 attribution, although model simulations diverge in some aspect, particularly for the
12 impacts of climate change and LCC, which suggests an area for future model
13 improvements. Overall, the described LAI trends represent a significant alteration of
14 the productive capacity of terrestrial vegetation through anthropogenic influences.

15

16 **Methods**

17 Methods and any associated references are available in the online version of the paper.

18

19 Received XX; accepted XX; published online XX

20

21 **References**

22

- 23 1 Peters, G. P. *et al.* The challenge to keep global warming below 2°C. *Nature Clim.*
24 *Change* **3**, 4-6 (2013).

- 1 2 Ciais, P. *et al.* *Climate Change 2013: The Physical Science Basis. Contribution of*
2 *Working Group I to the Fifth Assessment Report of the Intergovernmental Panel*
3 *on Climate Change* (eds T.F. Stocker *et al.*) Ch. 6, 465–570 (Cambridge University
4 Press, 2013).
- 5 3 Myneni, R. B., Keeling, C. D., Tucker, C. J., Asrar, G. & Nemani, R. R. Increased
6 plant growth in the northern high latitudes from 1981 to 1991. *Nature* **386**, 698-
7 702 (1997).
- 8 4 Pan, Y. *et al.* A large and persistent carbon sink in the world's forests. *Science* **333**,
9 988-993 (2011).
- 10 5 Xu, L. *et al.* Temperature and vegetation seasonality diminishment over northern
11 lands. *Nature Clim. Change* **3**, 581-586 (2013).
- 12 6 Los, S. O. Analysis of trends in fused AVHRR and MODIS NDVI data for 1982-
13 2006: indication for a CO₂ fertilization effect in global vegetation. *Glob.*
14 *Biogeochem. Cycles* **27**, 318-330 (2013).
- 15 7 Mao, J. F. *et al.* Global latitudinal-asymmetric vegetation growth trends and their
16 driving mechanisms: 1982-2009. *Remote Sens-Basel* **5**, 1484-1497 (2013).
- 17 8 Piao, S. *et al.* Detection and attribution of vegetation greening trend in China over
18 the last 30 years. *Glob. Change Biol.* **21**, 1601-1609 (2015).
- 19 9 Wang, X. H. *et al.* A two-fold increase of carbon cycle sensitivity to tropical
20 temperature variations. *Nature* **506**, 212-215 (2014).
- 21 10 Malhi, Y. *et al.* Climate change, deforestation, and the fate of the Amazon. *Science*
22 **319**, 169-172 (2008).
- 23 11 Ukkola, A. M. *et al.* Reduced streamflow in water-stressed climates consistent
24 with CO₂ effects on vegetation. *Nature Clim. Change* **advance online publication**,
25 doi:10.1038/nclimate2831(2015).
- 26 12 Piao, S. L. *et al.* Evaluation of terrestrial carbon cycle models for their response to
27 climate variability and to CO₂ trends. *Global Change Biol* **19**, 2117-2132 (2013).
- 28 13 Allen, M. R. & Tett, S. F. B. Checking for model consistency in optimal
29 fingerprinting. *Clim. Dynam.* **15**, 419-434 (1999).
- 30 14 Norby, R. J. *et al.* Forest response to elevated CO₂ is conserved across a broad

- 1 range of productivity. *Proc. Natl. Acad. Sci. USA* **102**, 18052-18056 (2005).
- 2 15 Schimel, D., Stephens, B. B. & Fisher, J. B. Effect of increasing CO₂ on the
- 3 terrestrial carbon cycle. *Proc. Natl Acad. Sci. USA* **112**, 436-441 (2015).
- 4 16 Galloway, J. N. *et al.* Nitrogen cycles: past, present, and future. *Biogeochemistry*
- 5 **70**, 153-226 (2004).
- 6 17 Donohue, R. J., Roderick, M. L., McVicar, T. R. & Farquhar, G. D. Impact of CO₂
- 7 fertilization on maximum foliage cover across the globe's warm, arid
- 8 environments. *Geophys. Res. Lett.* **40**, 3031-3035 (2013).
- 9 18 Wong, S. C., Cowan, I. R. & Farquhar, G. D. Stomatal conductance correlates with
- 10 photosynthetic capacity. *Nature* **282**, 424-426 (1979).
- 11 19 Achard, F. *et al.* Determination of deforestation rates of the world's humid tropical
- 12 forests. *Science* **297**, 999-1002 (2002).
- 13 20 Gibson, L. *et al.* Primary forests are irreplaceable for sustaining tropical
- 14 biodiversity. *Nature* **478**, 378-381 (2011).
- 15 21 LeBauer, D. S. & Treseder, K. K. Nitrogen limitation of net primary productivity
- 16 in terrestrial ecosystems is globally distributed. *Ecology* **89**, 371-379 (2008).
- 17 22 Magnani, F. *et al.* The human footprint in the carbon cycle of temperate and boreal
- 18 forests. *Nature* **447**, 848-850 (2007).
- 19 23 Canadell, J. G. & Schulze, E. D. Global potential of biospheric carbon
- 20 management for climate mitigation. *Nat. Commun.* **5**, 5282-5282 (2014).
- 21 24 Goulding, K. W. T. *et al.* Nitrogen deposition and its contribution to nitrogen
- 22 cycling and associated soil processes. *New Phytol.* **139**, 49-58 (1998).
- 23 25 Holland, E. A., Braswell, B. H., Sulzman, J. & Lamarque, J. F. Nitrogen deposition
- 24 onto the United States and western Europe: Synthesis of observations and models.
- 25 *Ecol. Appl.* **15**, 38-57 (2005).
- 26 26 Hansen, M. C. *et al.* High-resolution global maps of 21st-century forest cover
- 27 change. *Science* **342**, 850-853 (2013).
- 28 27 Mueller, T. *et al.* Human land-use practices lead to global long-term increases in
- 29 photosynthetic capacity. *Remote Sens-Basel* **6**, 5717-5731 (2014).
- 30 28 Lehner, B. & Döll, P. Development and validation of a global database of lakes,

- 1 reservoirs and wetlands. *J. Hydrol.* **296**, 1-22 (2004).
- 2 29 van der Werf, G. R. *et al.* Global fire emissions and the contribution of
- 3 deforestation, savanna, forest, agricultural, and peat fires (1997-2009). *Atmos.*
- 4 *Chem. Phys.* **10**, 11707-11735 (2010).

5

6

Accepted manuscript

1 **Additional information**

2 Supplementary information is available in the online version of the paper. Reprints and
3 permissions information is available online at www.nature.com/reprints.

4 Correspondence and requests for materials should be addressed to S. P.

5

6 **Acknowledgements**

7 This study was supported by the Strategic Priority Research Program (B) of the Chinese
8 Academy of Sciences (Grant XDB03030404), National Basic Research Program of
9 China (Grant 2013CB956303), National Natural Science Foundation of China (Grant
10 41530528), the 111 Project (Grant B14001), and the European Research Council
11 Synergy grant ERC-SyG-610028 IMBALANCE-P. We thank all people and institutions
12 who provide data used in this study, in particular, the TRENDY modelling group. RBM
13 is funded by NASA Earth Science. JGC thanks the support from the Australian Climate
14 Change Science Program. AA and TAMP acknowledge support through EC FP7 grants
15 LUC4C (Grant 603542) and EMBRACE (Grant 282672) and the Helmholtz
16 Association ATMO programme, YPW thanks for CSIRO strategic funding for CABLE
17 science, EK was funded by ERTDF (S10) from the Ministry of Environment, Japan.
18 JFM is supported by the US Department of Energy (DOE), Office of Science,
19 Biological and Environmental Research. Oak Ridge National Laboratory is managed
20 by UT-BATTELLE for DOE under contract DE-AC05-00OR22725.

21

22

23

1 **Author contributions**

2 S. P., R. B. M. and Z. Z. designed the study. Z. Z. performed the analysis; Z. Z., S. P.,
3 J. G. C., P. C., and R. B. M. drafted the paper. Z. Z., M. H., Z. Z., C. C., Y. L., H. Y., X.
4 W., X. L., Y. P., Y. L., R. L. and Z. X. collected data and prepared figures; S.S., P. F., A.
5 A., B. D. S., B. P., C. K., E. K., J. M., J. P., L. C., N. V., N. Z., S. P., S. Z., T. P., and Y.
6 W. ran the model simulations. All authors contributed to the interpretation of the results
7 and to the text.

8

9 **Competing financial interests**

10 The authors declare no competing financial interests.

Accepted manuscript

1 **Figure Legends**

2 **Figure 1.** The spatial pattern of trends in growing season integrated LAI derived from
3 three remote sensing data (a) GIMMS LAI3g, (b) GLOBMAP LAI and (c) GLASS LAI.
4 All data sets cover the period 1982 to 2009. Regions labeled by black dots indicate
5 trends that are statistically significant (Mann-Kendal test, $p < 0.05$). (d) Probability
6 density function of LAI trends for GIMMS LAI3g, GLASS LAI, GLOBMAP LAI and
7 the average of the three remote sensing data sets (AVG OBS).

8
9 **Figure 2.** (a) Interannual changes in anomalies of growing season integrated leaf area
10 index (LAI) estimated by multi-model ensemble mean (MMEM) with all drivers
11 considered (blue line) and average of the three remote sensing data (red line) for the
12 period 1982 to 2009, and interannual changes in anomalies of LAI of GIMMS LAI3g
13 (green line) for the period 1982 to 2014. The shaded area shows the intensity of El
14 Niño-Southern Oscillation (ENSO) as defined by the multivariate ENSO Index. The
15 black dash lines label the sensor changing time of the AVHRR satellite series. Two
16 volcanic eruptions (El Chichón eruption and Pinatubo eruption) were labeled in brown
17 dash lines. (b) Best estimates of the scaling factors of CO₂ fertilization effects, climate
18 change effects and simulated LAI under the four scenarios and their 5-95% uncertainty
19 range from optimal fingerprint analyses of global LAI for 1982-2009. (c) Trend in
20 global averaged LAI derived from satellite observation (OBS) and modeled trends
21 driven by rising CO₂, climate change (CLI), nitrogen deposition (NDE) and land cover
22 change (LCC) using the Mann-Kendal test. Error bars show the standard deviation of

1 trends derived from satellite data and model simulations. Two asterisks indicate that the
2 trend is statistically significant ($p < 0.05$).
3

4 **Figure 3.** The spatial distribution pattern of the trend in growing season integrated LAI
5 (a, b), its primary driving factors (c) and the latitudinal area fraction of the driving
6 factors (d) for the period 1982 to 2009. LAI trends were derived (a) from average of
7 GIMMS, GLOBMAP and GLASS LAI and (b) from multi-model ensemble mean with
8 all drivers considered; Regions labeled by dots have trends that are statistically
9 significant ($p < 0.05$). The trend is calculated and evaluated using the Mann-Kendal test
10 at 5% significance level. (c) The dominant driving factor is defined as the driving factor
11 that contributes the most to the increase (or decrease) in LAI in each vegetated grid-
12 cell. The driving factors include rising CO₂ (CO₂), climate change (CLI), nitrogen
13 deposition (NDE), land cover change (LCC) and other factors (OF), the latter being
14 defined by the non-modeled fraction of observed LAI trend (see text). Prefixed '+' of
15 driving factors indicate their positive effect on LAI trends, while '-' indicate negative
16 effect. (d) Fractional area of vegetated land in 15° latitude bands (90°N-60°S) attributed
17 to different factors. The fraction of vegetated area (%) that dominantly driven by each
18 factor was labeled on top of the bar.

19
20
21
22

1 **Methods**

2 The growing season integrated leaf area index was used as a proxy of vegetation growth
3 in this study. We identified the growing season for each $0.5^{\circ} \times 0.5^{\circ}$ grid cell of global
4 vegetated area utilizing GIMMS LAI3g data sets and freeze/thaw data sets. The
5 growing season was first determined from the GIMMS LAI3g data set³⁰ using Savitzky-
6 Golay filter and then refined by excluding the ground-freeze period identified by the
7 Freeze/Thaw Earth System Data Record³¹. In particular, the growing season of
8 evergreen broadleaf forests was set to 12 months and starts in January. All the satellite
9 observed leaf area products and leaf area index outputs of ecosystem models were first
10 aggregated to $0.5^{\circ} \times 0.5^{\circ}$ spatial resolution and then composited to annual growing
11 season integrated leaf area index data.

12
13 Three satellite-observed leaf area index products (GIMMS LAI, GLOBMAP LAI and
14 GLASS LAI) were used to analyze the changes in global vegetation for the period 1982
15 to 2009. We used a nonparametric trend test technique (Mann-Kendall test) to evaluate
16 trends in growing season integrated leaf area index derived from the three satellite LAI
17 products at the 95% significance level. We analyzed trends in LAI at pixel level, global
18 level and continental level. When we tested trends in LAI at global and continental
19 scales, we calculated the mean of LAI values of all the pixels in the specific region,
20 weighting by the area of each pixel.

21
22 Ten ecosystem models were used to analyze the relative contributions of external

1 driving factors to trends in global vegetation growth during 1982-2009. We performed
2 4 experimental simulations to evaluate the relative contribution of four main driving
3 factors, i.e. CO₂ fertilization, climate change, nitrogen deposition and land cover
4 change, to the global vegetation trends: (S1) varying CO₂ only, (S2) varying CO₂ and
5 climate, (S3) varying CO₂, climate and nitrogen deposition and (S4) varying CO₂,
6 climate and land cover change. S1, S2-S1, S3-S2 and S4-S2 were used to evaluate the
7 effects of CO₂ fertilization, climate change, nitrogen deposition and land cover change
8 to vegetation growth, respectively (see Section S7).

9
10 We used an optimal fingerprint method¹³ to detect the signals of CO₂ fertilization,
11 climate change, nitrogen deposition and land cover change effects simulated by
12 ecosystem models at global scales. The optimal fingerprint expresses the observation
13 (Y) as a linear combination of scaled (β_i) responses to external driving factors (x_i), and
14 internal variability (ε): $Y = \sum_{i=1}^n \beta_i x_i + \varepsilon$. The scaling factors (β_i) are estimated based
15 on the total least square method to adjust the amplitude of the responses of LAI to each
16 driving factors. We regressed the satellite observed LAI against responses of vegetation
17 growth (expressed as LAI) to elevated atmospheric CO₂, climate change, nitrogen
18 deposition and land cover change estimated by multi-model ensemble mean simulations
19 of 10 ecosystem models. We also performed similar analysis for the simulated LAI
20 under scenarios S1, S2, S3 and S4. These regressions provide best-estimate linear
21 combinations of signals simulated by ecosystem models. The coefficients of the signals
22 are the scaling factors (β_i). A residual consistency test was introduced to check the

consistency between the residuals of satellite observed LAI and best-estimate combinations of signals and the assumed internal LAI variability¹³. The overall statistical model was considered suitable only if the residual consistency test passed at 95% significance level. If the 95% confidence interval of the estimated scaling factor lies above zero, the signal of the corresponding driving factor is detected. And the model simulations are suitable for attribution if the 95% confidence interval contains 1.

7

8 **References**

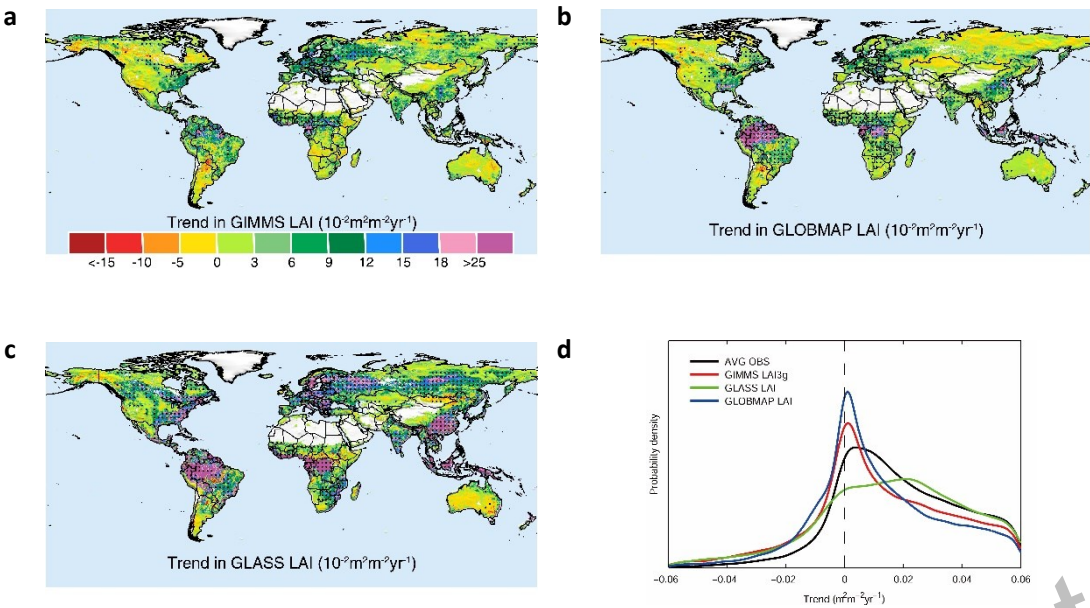
9

- 10 30 Zhu, Z. C. *et al.* Global data sets of vegetation leaf area index (LAI)3g and fraction
11 of photosynthetically active radiation (FPAR)3g derived from global inventory
12 modeling and mapping studies (GIMMS) normalized difference vegetation index
13 (NDVI3g) for the period 1981 to 2011. *Remote Sens-Basel* **5**, 927-948 (2013).
- 14 31 Kim, Y., Kimball, J. S., McDonald, K. C. & Glassy, J. Developing a global data
15 record of daily landscape freeze/thaw status using satellite passive microwave
16 remote sensing. *IEEE T. Geosci. Remote* **49**, 949-960 (2011).

17

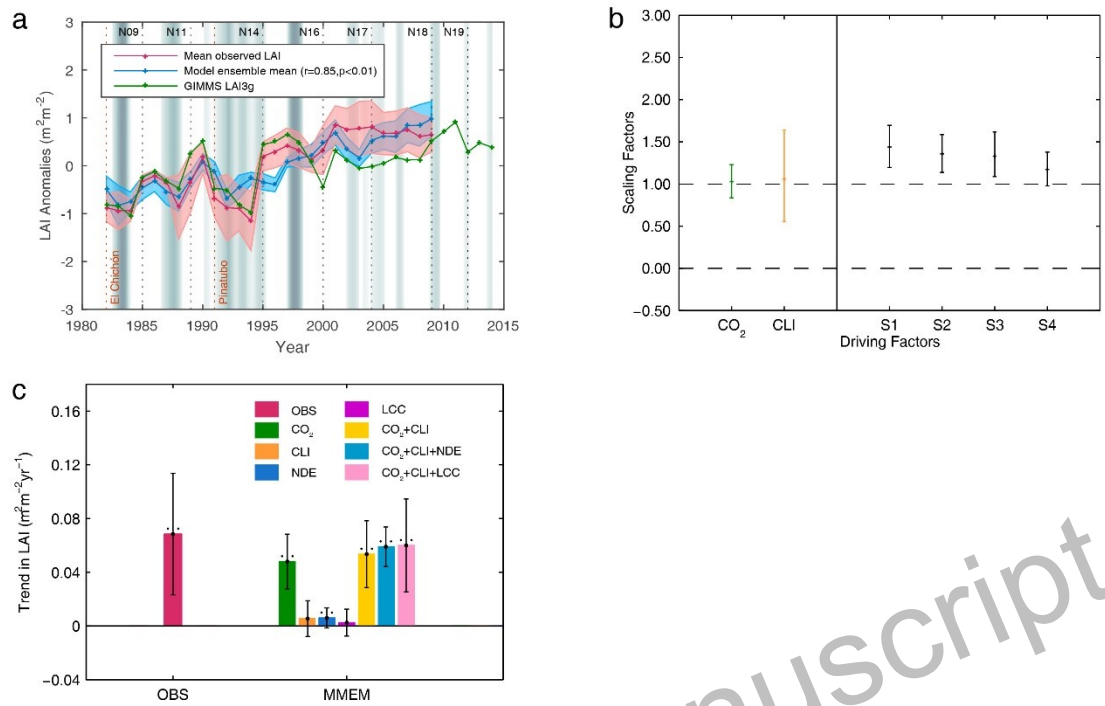
18

1 **Figure 1**



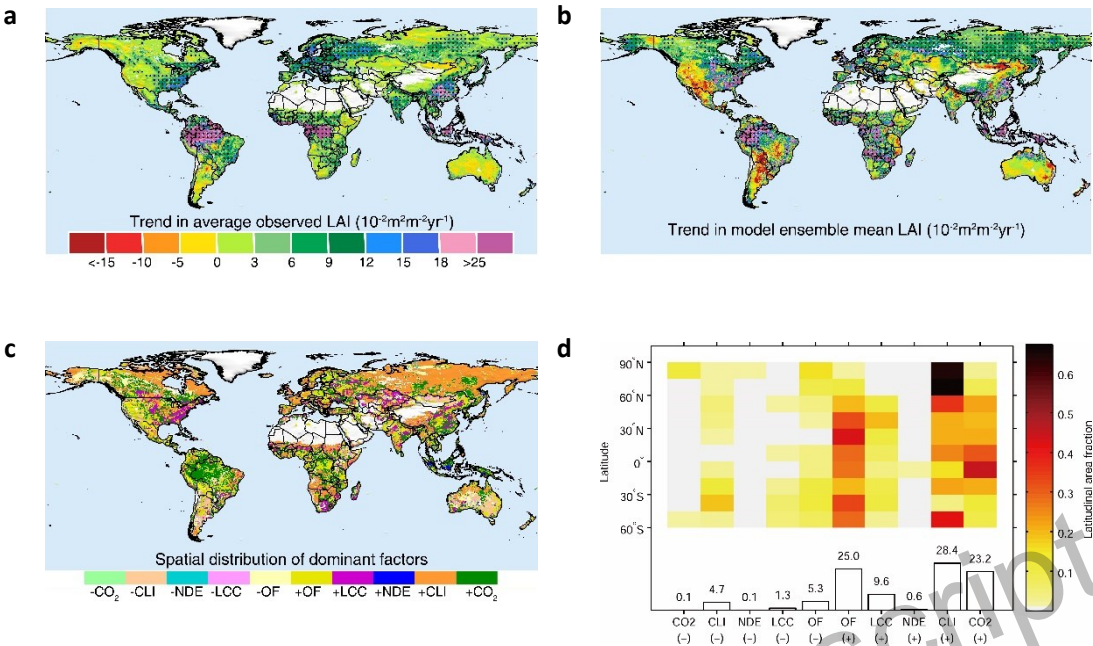
2
3

1
2 **Figure 2**



1 **Figure 3**

2



3

4